crystals

MDPI

Article

The Influence of Substitutional Defects of Transition Metal Elements on the Stability and Thermal Properties of Al at Finite Temperatures: A First-Principles Study

Tuo Ye [1,2], Lan Lin [1,2], Zixiong Ruan [1,2], Touwen Fan [1,2,3,*], Yuanzhi Wu [1,2] and Dongchu Chen [3,*]

[1] Research Institute of Automobile Parts Technology, Hunan Institute of Technology, Hengyang 421002, China; 2017001002@hnit.edu.cn (T.Y.); linlain123@163.com (L.L.); ruan_625627@163.com (Z.R.); 2013001767@hnit.edu.cn (Y.W.)
[2] College of Science, Hunan Institute of Technology, Hengyang 421002, China
[3] School of Material Science and Hydrogen Energy Engineering, Foshan University, Foshan 528001, China
* Correspondence: fantouwen@hotmail.com (T.F.); chendc@fosu.edu.cn (D.C.)

Abstract: Based on first-principles calculations, the effects of substitutional defects of the 3d–5d transition metal elements TM_{Al} on the stability and thermal conductivity of the aluminum matrix were investigated. The results show that with an increase in the atomic number of TM, the defect-forming energy E_f of TM_{Al} exhibits a periodic change feature, which depends on the valence electron configuration of the TM elements. The thermodynamic property parameters calculated with the Debye theory show that the addition of TM atoms does not change the stability of an Al system and can effectively reduce the thermal expansion coefficient of the material. But the equilibrium lattice constant a_0 of Al-TM_{Al} supercells changes very little. As the temperature increases, the relaxation time τ decreases, and both the electronic thermal conductivity κ_e and the total thermal conductivity κ decrease at the temperature range of 100–200 K, followed by a small increase or decrease. Because the lattice thermal conductivity κ_l is very small in the whole temperature range, the changes in electronic thermal conductivity and total thermal conductivity are basically the same. Moreover, when 1 at.% TM was added at both 300 K and 600 K, it was found that the influence of TM solute atoms on the thermal conductivity κ of Al was much greater than that of the second-phase particles. For solid solution atoms, Pd and Pt atoms have the greatest influence on the thermal conductivity of pure Al. This work is helpful for designing high-performance, heat-resistant Al-based alloys.

Keywords: first-principles calculations; defect formation energy; aluminum alloys; solid solution; thermal conductivity

check for updates

Citation: Ye, T.; Lin, L.; Ruan, Z.; Fan, T.; Wu, Y.; Chen, D. The Influence of Substitutional Defects of Transition Metal Elements on the Stability and Thermal Properties of Al at Finite Temperatures: A First-Principles Study. *Crystals* **2024**, *14*, 35. https://doi.org/10.3390/cryst14010035

Academic Editor: Andrey Prokofiev

Received: 4 December 2023
Revised: 20 December 2023
Accepted: 20 December 2023
Published: 27 December 2023

1. Introduction

For a long time, aluminum (Al) alloys have been widely used in vehicle and aerospace engineering industries due to their excellent physical and chemical properties, such as strong corrosion resistance, light weight, and high specific strength [1–6]. Nowadays, with the continuous development of technology, research related to high-performance Al alloys has ushered in a new era. In order to adapt to the progress of power electronics technology and the rapid development trend of 5G communication-network-related equipment, higher requirements are put forward for heat dissipation, creep resistance, and thermal conductivity. Moreover, these improved properties also make the Al-based alloys possess potential applications in computer heat sinks, automobile engine blocks, cylinder heads, communication base station radiators, overhead transmission wires, and other equipment [7–9]. However, the limited creep resistance and thermal conductivity of Al alloys greatly hinders their application at high temperatures. Fortunately, in the past few decades, related researchers have found that by adding appropriate transition elements (TMs) and rare earth elements (REs) to Al alloys, the $L1_2$ ordered binary precipitated phases can be produced with the appropriate heat treatment, namely, Al_3TM and Al_3RE intermetallic compounds. These binary intermetallics have excellent mechanical properties such as high specific strength, good elastic properties, and plasticity [10–12], as well as excellent physical properties such as a high melting point, good oxidation resistance, good thermal stability, and low mass density [13–25], thereby improving the creep resistance and thermal conductivity of Al alloys even at high temperatures.

The addition of RE elements will form a complex second phase with Fe, Si, and other elements in the alloy and promote precipitation in the form of Al_3RE, so that the element will change into the precipitation state, which is conducive to the improvement of electrical conductivity. At the same time, the formed second-phase particle Al_3RE can effectively restrict the dislocation and sub-grain boundary and hinder the grain growth, and thus, increase the recrystallization temperature to improve the heat resistance of the Al-based materials. Al_3Sc and Al_3Y are of great significance in providing superplastic ductility for Al-based alloys [26–28]. Jahnátek [29] et al. have shown that the presence of Al_3Sc precipitation increases the creep resistance of coarse-grained Al-Mg-Sc ternary alloys. It has also been shown that the uniform distribution of Al_3Sc effectively refines the grain boundaries and is beneficial to the thermal stability of the refined grain size [30,31]. Compared with Al_3Li, Al_3Sc has higher structural stability and stronger reinforcement [32].

On the other hand, related studies have shown that Al_3Ti has excellent properties of high melting point (1610 K), relatively low density (3.4 g/cm^3) [33], high Young's modulus (216 GPa) [34], and strong oxidation resistance [35]. Compared with $D0_{22}$ Al_3Ti, the compressive strain of $L1_2$ type Al_3Ti at high temperature has a significant promoting effect [36,37]. At the same time, Al_3Zr particles with an $L1_2$ structure have good thermal stability, which can effectively prevent dislocation and sub-grain boundary migration and increase the recrystallization temperature and thus improve the heat resistance of the Al-based material. Guan et al. [38] found that Al_3(Zr, Sc) complex precipitates could further improve the mechanical properties and the electrical conductivity of Al-based alloy cables. The appropriate addition of Zr in Al can improve the heat resistance of Al alloys; proper addition of Er can not only improve the heat resistance of the Al-based alloy, but also react with Si and Fe to purify the alloy [39]. When 0.1 wt % Er and 0.04 wt % Zr were added to Al alloys, it was found that the electrical conductivity and heat resistance of the Al alloys were good [40,41]. Relevant studies have confirmed that the introduction of the TM element Nb successfully tunes the microstructure and properties of Al alloys and enables the formation of Al_3Nb to make the matrix have good oxidation resistance [21,42–46]. Tzeng et al. [47] found that metastable $L1_2$-Al_3Sc can improve the strength of Al alloys by inhibiting recrystallization and refining grains [48]. There have been many studies on the precipitation of the $L1_2$-Al_3TM phase of transition elements, especially Sc elements, but the high cost of Sc hinders the wide application of the Al_3Sc phase in the strengthening process of Al alloys. Because the Al_3RE phase with the $L1_2$ structure has been comprehensively studied, this study turns its attention to the $L1_2$-Al_3TM phase, in the hope of exploring feasible candidates for cheaper TM elements that can replace the Sc element.

A large number of studies have shown that the improvement of Al alloy properties is mainly due to the action of the second-phase particles. Taking Al_3Sc as an example, the second-phase particle can act as the heterogeneous nucleation center of grains during the solidification of the alloy liquid and play a role in weakening or even eliminating dendrites. At the same time, the recrystallization temperature of the alloy can be increased by inhibiting the nucleation and growth of recrystallization grains during the process of thermal deformation and heat treatment, and the dislocation movement and sub-grain boundary migration and merger can be prevented to improve the alloy strength. It can be seen that the improvement of the second phases on performance of the Al alloy is crucial.

The crystal structure and thermophysical properties can be further improved by doping TM elements [49–52]. However, due to the dissolution of TM in Al, forming TM_{Al}, it acts as the center of electron scattering, resulting in a great reduction in thermal conductivity. Vandersluis et al. reported that the thermal conductivity of the cylinder head T7 sample was improved by the dissipation of solute atoms in the Al matrix that acted as electron-scattering centers [53]. Therefore, point defects, especially substitutional impurity defects, are also important factors affecting the mechanical and thermodynamic properties of Al alloys at high temperatures, which is a difficult problem to be solved by the majority of scientific researchers. At present, although a large number of experimental and theoretical studies have been carried out on Al_3TM phases, the effects of point defects in TM_{Al} on the thermal conductivity of Al alloys are rarely considered, and a systematic database is lacking. In recent years, with the unprecedented development of computer technology, computational materials science has formed a research upsurge, which not only has laid the foundation data for the experimental research, but also provides a new way of thinking for material research. Its theoretical research methods have gradually matured and can provide a theoretical basis for the optimal design of material properties and basic data support for production and application. In this paper, based on the first-principles calculations, the defect formation energy of substitutional impurities TM_{Al} in Al is calculated and the influence of TM solute atoms on the thermal conductivity of an Al matrix at various temperatures and concentrations is further analyzed. It is hoped that the research on high thermal conductivity of Al alloys can provide further basis and guidance.

2. Computational Detail

The first-principles calculation software Vienna ab initio simulation package (VASP) [54] code, based on density function theory [55], was adopted. The Perdew–Burke–Ernzerhof (PBE) version of the generalized gradient approximation (GGA) [56] was used to deal with the exchange-correlation functional, which can more accurately describe the energy of the structure and improve the convergence speed. In this work, the effects of substitution point defects TM_{Al} (including 3d (Sc-Zn), 4d (Y-Cd), and 5d (Hf-Hg)) on the stability and thermal conductivity of Al were investigated. A 3 × 3 × 3 supercell model with 108 atoms was employed for the study, and the PAW_GGA pseudopotentials of Al, Sc-Zn, Y-Nb_sv, and Mo-Hg were used during the relaxation calculations. The cutoff energy of 400 eV for plane wave was set to ensure high accuracy of calculation, and the Brillouin zone sampling was considered using the gamma-centered Monkhorst–Pack method [57] with 4 × 4 × 4 k-point meshes. The electronic self-consistence convergency criterion for electron iteration was 10^{-6} eV/atom; the ground-state geometries were relaxed via conjugate gradient (CG) minimization until the Hellman–Feynman forces [58] on each atom were less than 0.01 eV/Å. To calculate the influence of substitutional point defects TM_{Al} on the electronic transport of Al alloys, the electronic Boltzmann transport equation (BTE) was solved through performing in the BoltzTraP2 code [59], and a larger k-mesh with 6 × 6 × 6 and cutoff energy of plane wave basis of 500 eV were used. Thermodynamic properties were calculated using the Debye theory [60], and lattice thermal conductivity (LTC) was calculated using the Slack equation based on the Debye model [61–63].

3. Result and Discussion

3.1. Defective Formation Energy

In order to study the stability of defects TM_{Al} in the Al matrix, we first calculated the lattice constant a_0 of Al-TM_{Al} and the defect formation energy E_f of TM_{Al}. Generally speaking, there are two kinds of defects in the Al matrix that have a great influence on its performance, namely, vacancy and substitutional impurity defects. The calculation formula of defect formation energy is as follows [64,65]:

$$\Delta E_{\mathrm{f}} = E_{\mathrm{def}}^{\mathrm{total}} - E_{\mathrm{per}}^{\mathrm{total}} - \sum_{\mathrm{i}} n_{\mathrm{i}}\mu_{\mathrm{i}} \tag{1}$$

where $E_{\mathrm{def}}^{\mathrm{total}}$ and $E_{\mathrm{per}}^{\mathrm{total}}$ are the total energies of defective and perfective supercells, respectively; n_{i} is the coefficient of increase ($n_{\mathrm{i}} > 0$) or decrease ($n_{\mathrm{i}} < 0$) in the number of atoms caused by the defect; and μ_i is the chemical potential corresponding to a specific type, which is derived from the energy of a single atom in the most stable system, from the database calculated with the VASP package [54]. $\sum_i n_i \mu_i$ is the total variation chemical energy as a result of the defects.

Following the rule of thermal laws, it should be ensured that the chemical potential μ_i of the solute atom defects TM_{Al} is less than that of the bulk chemical potential μ_{bulk} of pure TM to avoid an accumulation of TM, as follows:

$$\mu_i - \mu_{bulk} \leq 0 \quad (2)$$

Figure 1a illustrates the computational model of the Al-TM_{Al} solid solution, in which one TM element is placed in the center of the crystal, corresponding to a concentration of ~1 at.%, and the calculated results of the lattice constant a_0 of the Al-TM_{Al} supercell and the defect formation energy of TM_{Al} in Al are shown in Table 1. Taking Al-W as an example, the lattice constant and atomic position information of the optimized structure have been placed in Table S6. It can be seen that the equilibrium lattice constant a_0 of the supermonomer Al-TM_{Al} is in good agreement with the reported theoretical predictions and experimental values, indicating that the calculation method has high accuracy. The equilibrium lattice constant a_0 changes very little, implying that the TM elements can hardly change the volume of Al alloys. The calculated defect formation energy ΔE_f of TM_{Al} varies with the atomic number. To clearly present the variations feature, we have further plotted the ΔE_f as a function of the atomic number of the TM element in Figure 1b. It is shown that the ΔE_f of TM_{Al} in the Al matrix shows a similar changing trend for 3d–5d cycles, and they all present a "W" shaped periodic changing feature.

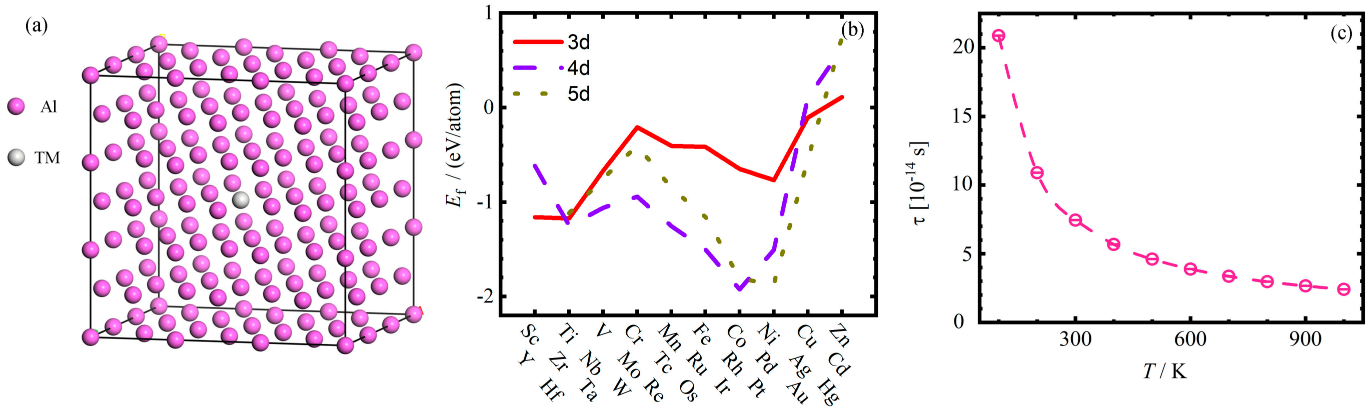

Figure 1. (**a**) The computational model for AlTM_{Al} solid solution, (**b**) the defective formation energy E_f of TM_{Al} as a function of atomic number, and (**c**) the relaxation time of Al again to temperature.

The positive values of ΔE_f indicate the difficulty of the dissolution of atoms in the Al matrix. From this point of view, the elements Zn, Cd, Ag, and Hg are hard to form Al-TM binary solid solutions. Furthermore, it is interesting to note that the formation energy differences ΔE_f of the replacement defects TM_{Al} of the later elements (3d (Ni-Zn), 4d (Rh-Cd), and 5d (Pt-Hg)) are significantly higher than those of the preceding TM elements, which means that these elements are also more difficult to dissolve in the Al matrix. From the above results, it is reasonable to speculate that the valence electrons of elements determine the defect formation energy ΔE_f and equilibrium lattice constant a_0 of Al-TM_{Al} binary solid solutions. However, it should be noted that the defect formation enthalpy values of group IB and group IIB are inclined to or higher than 0, indicating that the substitutional defects formed by these two subgroup elements in the aluminum matrix are difficult.

Table 1. The calculated equilibrium lattice constants a_0 (Å) of Al-TM$_{\mathrm{Al}}$ solid solution and defective formation energy ΔE_{f} (eV) of TM$_{\mathrm{Al}}$ in Al.

Systems	E_{f}	a_0
Al	--	4.039; 4.039 [66]; 3.983 [66]; 4.032 [67]
V_{Al}	0.68; 0.67 [66]; 0.73 [66]; 0.67 [68] 0.54 [69]; 0.70 [69]	4.035
Sc$_{\mathrm{Al}}$	−1.16	4.045
Ti$_{\mathrm{Al}}$	−1.17	4.038
V$_{\mathrm{Al}}$	−0.67	4.035
Cr$_{\mathrm{Al}}$	−0.21	4.032
Mn$_{\mathrm{Al}}$	−0.41	4.032
Fe$_{\mathrm{Al}}$	−0.41	4.032
Co$_{\mathrm{Al}}$	−0.65	4.031
Ni$_{\mathrm{Al}}$	−0.76	4.033
Cu$_{\mathrm{Al}}$	−0.10	4.035
Zn$_{\mathrm{Al}}$	0.11	4.038
Y$_{\mathrm{Al}}$	−0.62	4.052
Zr$_{\mathrm{Al}}$	−1.25	4.044
Nb$_{\mathrm{Al}}$	−1.06	4.039
Mo$_{\mathrm{Al}}$	−0.94	4.036
Tc$_{\mathrm{Al}}$	−1.26	4.033
Ru$_{\mathrm{Al}}$	−1.50	4.032
Rh$_{\mathrm{Al}}$	−1.92	4.033
Pd$_{\mathrm{Al}}$	−1.51	4.036
Ag$_{\mathrm{Al}}$	0.10	4.039
Cd$_{\mathrm{Al}}$	0.63	4.045
Hf$_{\mathrm{Al}}$	−1.12	4.043
Ta$_{\mathrm{Al}}$	−0.75	4.039
W$_{\mathrm{Al}}$	−0.40	4.035
Re$_{\mathrm{Al}}$	−0.85	4.033
Os$_{\mathrm{Al}}$	−1.16	4.032
Ir$_{\mathrm{Al}}$	−1.81	4.033
Pt$_{\mathrm{Al}}$	−1.87	4.034
Au$_{\mathrm{Al}}$	−0.55	4.039
Hg$_{\mathrm{Al}}$	0.74	4.045

3.2. The Thermodynamic Properties

Based on the quasi-harmonic Debye model [70–72] in the Gibbs2 program, the thermodynamic properties of the materials were calculated at 0 Pa and the temperature range was 0–1000 K [73]. According to the Debye theory [60], a crystal quasi-harmonic vibration model was obtained, and the Debye function Θ_D was calculated to analyze the Debye cutoff frequency ω_D [61–63,74,75]:

$$\Theta_D = \frac{h}{2\pi\kappa_B}\omega_D \tag{3}$$

where h is Planck's constant (6.63×10^{-34} J/s) and κ_B is Boltzmann's constant (1.38×10^{-23} J/K). ω_D can be expressed using Debye's sound velocity ν_D as:

$$\frac{\omega_D}{\nu_D} = \left(\frac{6\pi^2}{V}\right)^{1/3} \tag{4}$$

where V is the volume of the solid in the steady state. But the speed of sound has three different types and is anisotropic. For isotropic media, Anderson [76] expressed the mean crystal sound velocity at low temperature as:

$$\frac{1}{\nu_D^3} = \frac{1}{3}\left(\frac{1}{\nu_L^3} + \frac{2}{\nu_S^3}\right) \tag{5}$$

and

$$\nu_L = \sqrt{\frac{L}{\rho}}, \quad \nu_S = \sqrt{\frac{S}{\rho}} \tag{6}$$

where ν_L and ν_S are the longitudinal and transverse sound velocities, respectively, and ρ is the density of the material. The Poisson's ratio ν of the crystal can be expressed as:

$$\nu = \frac{3B - 2G}{2(3B + G)} \tag{7}$$

where B and G are the bulk modulus and shear modulus of the crystal, respectively.

According to Formulas (3)~(7), a simpler method for calculating ν_D and Θ_D can be obtained by calculating the transverse modulus S and longitudinal modulus L. The calculation is as follows:

$$L = \frac{3(1-\nu)}{1+\nu}B, \qquad S = \frac{3(1-2\nu)}{2(1+\nu)}B \tag{8}$$

Then, the ν_D can be obtained:

$$\nu_D = f(\nu)\sqrt{\frac{B}{\rho}} \tag{9}$$

$$f_\nu = \left\{\frac{1}{3}\left[\left[\frac{1+\nu}{3(1-\nu)}\right]^{\frac{3}{2}}\right] + 2\left[\left[\frac{2(1+\nu)}{3(1-2\nu)}\right]^{\frac{3}{2}}\right]\right\}^{-\frac{1}{3}} \tag{10}$$

This method has been proved to be suitable for obtaining a reasonable Debye sound velocity. Therefore, Θ_D can be obtained by combining the above formula:

$$\Theta_D = f_\nu \frac{h}{2\pi\kappa_B}\left(48\pi^5\right)^{\frac{1}{6}}\sqrt{\frac{r_0 B}{M}} \tag{11}$$

where the M is the atomic weight and r_0 is the equilibrium Wigner–Seitz radius.

The thermodynamic parameters of Gibbs free energy G, entropy S, coefficient of thermal expansion α, and the relevant formulas for calculating the constant volume specific heat capacity C_V can be further deduced from Formula (12):

$$F(V;T) = E(V) - \kappa_B T\left\{D\left(\frac{\Theta_D}{T}\right) - 3\ln\left[1 - e^{\left(\frac{-\Theta_D}{T}\right)}\right] + \frac{9}{8}\kappa_B\Theta_D\right\} \tag{12}$$

$$S = 3\kappa_B\left\{\left(\frac{4D\Theta_D}{3T} - In\left[1 - exp\left(\frac{-\Theta_D}{T}\right)\right]\right)\right\} \tag{13}$$

$$C_V = 3\kappa_B[4D\left(\frac{\Theta_D}{T}\right) - \frac{3\left(\frac{\Theta_D}{T}\right)}{e^{\frac{\Theta_D}{T}} - 1}] \tag{14}$$

$$\gamma_D = -\frac{\ln\partial\Theta_D}{\ln\partial InV}; \qquad a_T = \frac{\gamma C_V}{B_0 V} \tag{15}$$

The calculated results are shown as Figure 2. As we all know, the Gibbs free energy G can easily determine the direction and limit of the reaction, and the reduction in G in the reaction process is the maximum limit for the system to perform non-volume work. Both the Gibbs free energy G of all Al-TM solid solutions and Al matrices decrease with the increase in temperature, as seen in Figure 2a; the decrease in G in the reaction process is ~0.4 eV/atom, and the change trend is all the same. However, the Gibbs free energy G of Al-TM solid solutions (-3.7~-4.2 eV/atom) is slightly higher than that of Al (-3.7~-4.1 eV/atom), and the addition of TM keeps the system stable. In an isolated system, there is no energy exchange between the system and the environment, and the system always changes spontaneously in the direction of increasing the degree of disorder; that is, the system changes from an ordered state to a disordered state. It can be seen from Figure 2b that both the entropy S of the Al-TM solid solution and Al increase with the increase in temperature due to the more intense molecular motion caused by the increase in temperature, which further deviates from the stable state. The expansion α is one of the key properties of the thermodynamic properties of materials. It is commonly used to characterize the degree of thermal expansion of solid materials, that is, the change in material volume with temperature. Generally speaking, a rising temperature will increase the volume of materials, and materials with low expansion coefficients are expected to be applied in the field of high-precision instrument engineering. In Figure 2c, the coefficient of thermal expansion α at 1000 K was 5.6×10^{-5}. In addition to Al vacancy, the addition of Zn, Cd, and Hg solid solution atoms will slightly increase the degree of thermal expansion α, which may be due to the thermodynamic instability of Zn metal, while Cd metal is heated violently and Hg can rapidly swing at high temperatures, resulting in the addition of these elements to increase the coefficient of thermal expansion α of Al. However, the addition of other solvable atoms reduces the expansion coefficient of Al, indicating that the addition of TM elements is expected to make the Al alloy develop into high-temperature precision materials. Under the condition of constant volume, the heat absorbed by Al and Al-TM solid solutions at 0–1000 K for every 100 K increase was observed, and the results are shown in Figure 2d. According to the images, at 0–300 K, the constant volume specific heat capacity C_V increases exponentially with the increase in temperature, and the increment at this stage is about 23 $\mathrm{Jmol^{-1}K^{-1}}$. At the stage of 300–1000 K, the specific heat capacity at constant volume increases linearly with the increase in temperature, and the increment of this stage is only 2 $\mathrm{Jmol^{-1}K^{-1}}$. This shows that at the stage of 0–300 K, the material has completed most of the heat absorption.

All in all, according to the thermodynamic property parameters, the study shows that the addition of TM atoms does not change the system stability of Al and can effectively reduce the thermal expansion coefficient of the material, which provides support for the application of Al in the field of high-temperature precision instruments.

3.3. Thermal Conductivity

Understanding the heat conduction of materials can better measure their adiabatic and thermal conductivity properties to adapt to the rapid development of modern technologies such as electronics, artificial intelligence, and thermoelectricity. The importance of developing high-thermoelectric materials has become increasingly prominent, which puts forward higher requirements on the thermal conductivity of materials to improve the heat dissipation demand, thereby extending their service life and improving their operating efficiency [77,78]. Generally speaking, in metal systems, the interaction between electrons has a decisive influence on the thermal and electrical transport of materials, while the thermoelectric transport of phonons at medium and high temperatures is limited by electron-phonon scattering [79,80]. Therefore, the thermal conductivity block κ can be approximated by the composition of lattice thermal conductivity (LTC) κ_l and electron thermal conductivity (ETC) κ_e. That is to say, the total thermal conductivity (TC) formula is $\kappa = \kappa_e + \kappa_l$.

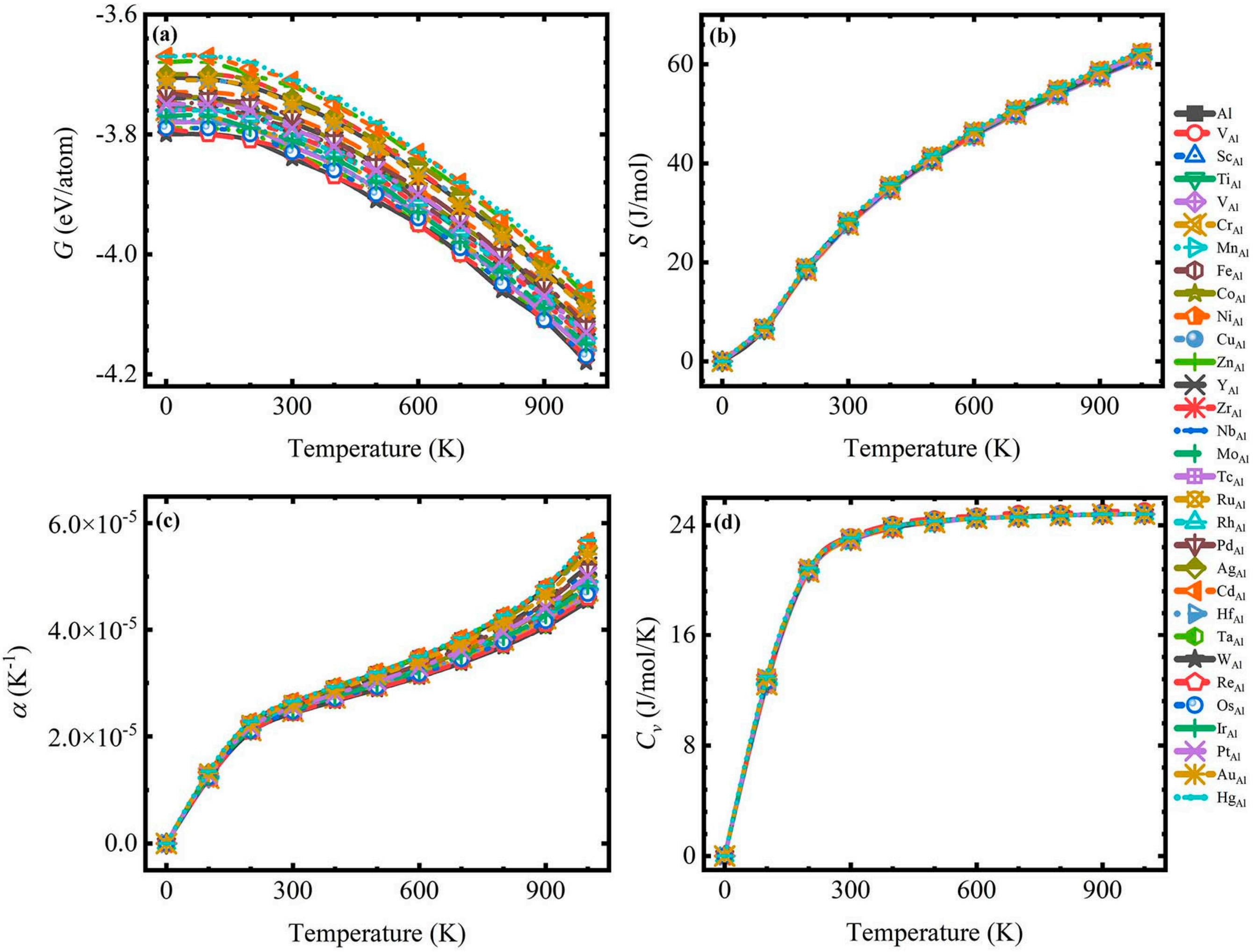

Figure 2. The calculated (**a**) Gibbs free energy G; (**b**) entropy S; (**c**) thermal expansion coefficient α; (**d**) constant volume specific heat C_V as a function of temperature for an Al matrix and Al-TM solid solution (including Al vacancy) at 0–1000 K.

In this paper, the lattice thermal conductivity κ_l is obtained by combining VASP with BoltzTraP and using Slack's model [81,82]. The calculated Debye temperature θ_α and Grüneisen parameter γ are both put into the Slack equation to obtain the lattice thermal conductivity κ_l [83]:

$$\kappa_l(\mathrm{T}) = \frac{0.849 \times 3\sqrt[3]{(4)}}{20\pi^3(1-0.154\gamma^{-1}+0.228\gamma^{-2})} \times \left(\frac{\kappa_B\theta_\alpha}{\hbar}\right)^2 \frac{\kappa_B M_{av} V^{\frac{1}{3}}}{\hbar\gamma^2} \times \frac{\theta_\alpha}{\mathrm{T}} \tag{16}$$

where V, M_{av}, κ_B, and $\hbar$ are the primitive cell volume, average atomic mass, Boltzmann constant, and reduced Planck constant, respectively.

Further, by using the Boltzmann transport theory [84–87], the expression of conductivity σ as a function of temperature can be given by the following formula:

$$\sigma_{\alpha\beta}(T,\mu) = \frac{1}{V}\int \sigma_{\alpha\beta}(\varepsilon)\left[-\frac{\partial f_0(T,\varepsilon,\ \mu)}{\partial\varepsilon}\right]d\varepsilon \tag{17}$$

where e, ε, f_0, and μ are the electronic charge, band energy, chemical potential, and the Fermi–Dirac distribution function, respectively.

The group velocity $v_\alpha(i,k)$ can be obtained from band structure calculations as

$$v_\alpha(i,k) = \frac{1}{\hbar}\frac{\partial \varepsilon_{i,k}}{\partial k_\alpha} \tag{18}$$

From the combination of Equations (4) and (5), the projected energy transport distribution tensor $\sigma_{\alpha\beta}$ can be expressed as

$$\sigma_{\alpha\beta}(\varepsilon) = \frac{\mathrm{e}^2}{\mathrm{N}}\sum\nolimits_{i,k} \tau_{i,k}\nu_\alpha(i,k)\nu_\beta(i,k)\frac{\delta(\varepsilon-\varepsilon_{i,k})}{\mathrm{d}\varepsilon} \tag{19}$$

where N, i, k, and $\nu_{\alpha,\beta}$ (i, k) are the number of the k-points, the band index, the wave vector, and the group velocity of the acoustic wave, respectively. Equation (19) is solved under constant relaxation time approximation (RTA) [84,85], and, for simplicity, we adopted a relaxation time of 10^{-13} as obtained by the experiment [88]. Near the Fermi level of the system, the chemical potential has an energy range of 0.09 Ry [85].

Then, we calculated the κ_e according to the Wiedemann–Franz law [89],

$$\kappa_\mathrm{e} = L\sigma T, \tag{20}$$

where

$$L = \frac{\pi^2\kappa_B^2}{3e^2} \tag{21}$$

where L is the Lorentz number, σ is the electrical conductivity, and T is the temperature in Kelvins.

The relaxation time τ in this study is calculated according to the formula τ = A × T^{-r}, where A is a proportional constant and r is the scaling factor [90–92]. Their fitted results are used in the present investigation for both pure Al and Al-TM$_\mathrm{Al}$ solid solutions, which is shown in Figure 1c. With the increase in temperature, the relaxation time decreases. Based on this basic assumption, the calculated values of κ_l, κ_e, and κ obtained from the above formula are shown in Table 2. The thermal conductivity of Al and Al-TM$_\mathrm{Al}$ solid solutions as a function of temperature and atomic number are shown in Figure 3a–f, respectively.

In order to explicitly exhibit the variation feature of LTC as a function of both temperature and atomic number, Figure 3a,c,e shows the calculated κ_l, κ_e, κ as a function of atomic number and Figure 3b,d,f presents the corresponding results as a function of temperature, respectively. The detail values are summarized in Supplementary Tables S1–S5. LTC κ_l changes with the atomic number at both 300 K and 600 K are illustrated in Figure 3a. It is seen that with the increase in atomic number, for 3d–5d TM elements, the variation trend of the LTC at 300 K and 600 K is the same, a trend of slow rising and then slow decline. But it is obvious that the LTC κ_l at 300 K is significantly higher than that at 600 K, in the range of ~5.16 Wm^{-1}K^{-1}. As is shown in Figure 3b, the LTC κ_l is roughly inversely proportional to temperature, consistent with the functional relationship in the literature. As is well known, the LTC mainly comes from the vibration of the atoms in the crystal lattice, and the larger the noise caused by the thermal movement of the atoms, the worse transportation ability the phonon of the metal material is. Compared with the values of one another, it is found that the numerical differences of the LTC κ_l decreases with increasing temperature. It can be found that the LTC κ_l of both defects containing Al-TM$_\mathrm{Al}$ and perfect Al supercells decreases sharply with the increase in temperature (0~600 K), and then the deceasing velocity slows down, but the variation range is only about 26.64 Wm^{-1}K^{-1}, far smaller the that of the ETC.

Table 2. The calculated κ_l, κ_e, and κ (units in $Wm^{-1}K^{-1}$) of TM_{Al} containing a perfect supercell at room temperature of 300 K.

	κ_l	κ_e	κ
Al	7.38 4.83 [93]	223.61	230.99 190.90 [93]; 240.00 [89]
V_{Al}	7.48	178.95	186.43
Sc_{Al}	7.71	176.13	183.85
Ti_{Al}	8.14	181.60	189.75
V_{Al}	8.22	177.43	185.65
Cr_{Al}	8.20	178.41	186.61
Mn_{Al}	8.15	176.13	184.28
Fe_{Al}	8.06	178.67	186.73
Co_{Al}	7.91	177.65	185.57
Ni_{Al}	7.69	183.41	191.10
Cu_{Al}	7.44	184.12	191.55
Zn_{Al}	7.28	205.54	212.82
Y_{Al}	7.53	161.69	169.21
Zr_{Al}	8.04	158.06	166.09
Nb_{Al}	8.24	158.30	166.54
Mo_{Al}	8.30	162.37	170.67
Tc_{Al}	8.25	153.81	162.06
Ru_{Al}	8.12	150.51	158.62
Rh_{Al}	7.92	153.73	161.65
Pd_{Al}	7.65	140.95	148.60
Ag_{Al}	7.33	144.98	152.30
Cd_{Al}	7.21	194.94	202.15
Hf_{Al}	7.97	175.14	183.10
Ta_{Al}	8.21	174.88	183.09
W_{Al}	8.28	162.70	170.98
Re_{Al}	8.20	158.10	166.30
Os_{Al}	8.11	151.66	159.76
Ir_{Al}	7.92	142.88	150.80
Pt_{Al}	7.67	115.51	123.19
Au_{Al}	7.34	127.02	134.36
Hg_{Al}	7.09	191.10	198.19

Comparing Figure 3c,e, it can be found that the relationship between the ETC κ_e and atomic numbers of TM are related to the position of the atoms in the periodic table. The ETC κ_e of all Al-TM_{Al} at 300 K and 600 K is nearly the same. For 3d transition elements, the ETC κ_e increases slowly from Sc to Cu, and then jumps to Zn by about 20 $Wm^{-1}K^{-1}$. Looking at the 4d and 5d TM elements, it is found that the ETC κ_e of Al-TM_{Al} solid solution is the smallest for Pd and Pt in the group VIII, and thus, with Pd and Pt as nodes, it first slowly decreases and then rapidly increases. In the same way, the total TC κ as a function of temperature and atomic number tends to be basically the same as the function of the ETC κ_e. According to Figure 3d, the calculated value of the ETC κ_e of the Al matrix increases fast from 203.34 $Wm^{-1}K^{-1}$ at 100 K to 217.81 $Wm^{-1}K^{-1}$ at 200 K, and then the increasing velocity decreases. On the contrary, the Al-TM_{Al} solid solutions show a decreasing trend in the temperature range of 100–200 K at first, and then they all show a small variation. Among them, the change in the ETC κ_e and the TC κ of Al-Zn_{Al} is the closest to that of Al, while the change in Al-Pt_{Al} is quite different from that of Al. At the same time, due to the small influence of LTC κ_l, the functional relationship between the TC κ and temperature, as is shown in the Figure 3f, is nearly the same as that of ETC κ_e, as illustrated in Figure 3d.

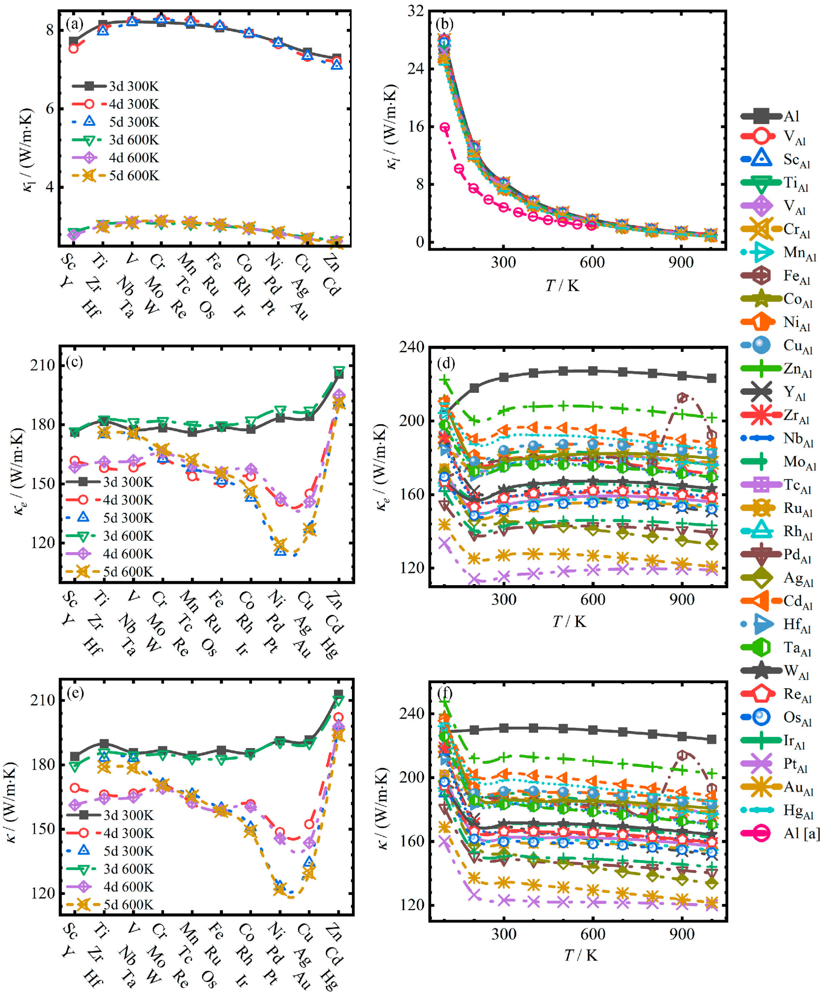

Figure 3. (**a**,**c**,**e**) show the calculated κ_l, κ_e, κ as a function of atomic number, and (**b**,**d**,**f**) denote the calculated κ_l, κ_e, κ as a function of temperature. Data from reference [93].

3.4. The Effect of 1 at.% TM Added on Thermal Conductivity

To quantitatively analyze the effects of second-phase particles L1$_2$-Al$_3$TM and TM solute on the TC κ of Al, 1 at.% TM defects as above two states added to the Al matrix were further investigated to quantitatively exhibit the trends of different elements on the thermal conductivity of the Al matrix at finite temperatures. The relationships between thermal conductivity κ and the atomic number of TM for Al-L1$_2$-Al$_3$TM phase and Al-TM$_{Al}$ systems when 1 at.% TM is added at 300 K and 600 K are shown in Figure 4a,b, respectively. Meanwhile, the thermal conductivity κ of the Al matrix at 300 K and 600 K is provided for comparing. Specifically, Figure 4a,b shows that the thermal conductivity κ of TM solute atoms at 300 K and 600 K as a function of atomic number is consistent with Figure 3f. It is found that when 1 at.% TM is added, the thermal conductivity κ of the second-phase particles remains almost at a horizontal level for all three 3d–5d periodic TM elements. In 3d (Sc-Zn), the thermal conductivity κ of Al-TM$_{Al}$ increases with the increase in atomic number, the change is relatively stable, and the maximum thermal conductivity reduces in the Al matrix by no more than 5%. In 4d (Y-Cd) and 5d (Hf-Hg), the thermal conductivity κ decreases with the increase in atomic number, from about 30% at the beginning to about 50% at the lowest, and finally rises to 15%. Moreover, the lowest values appear in Pd and Pt for 4d and 5d, respectively, and then the values increase.

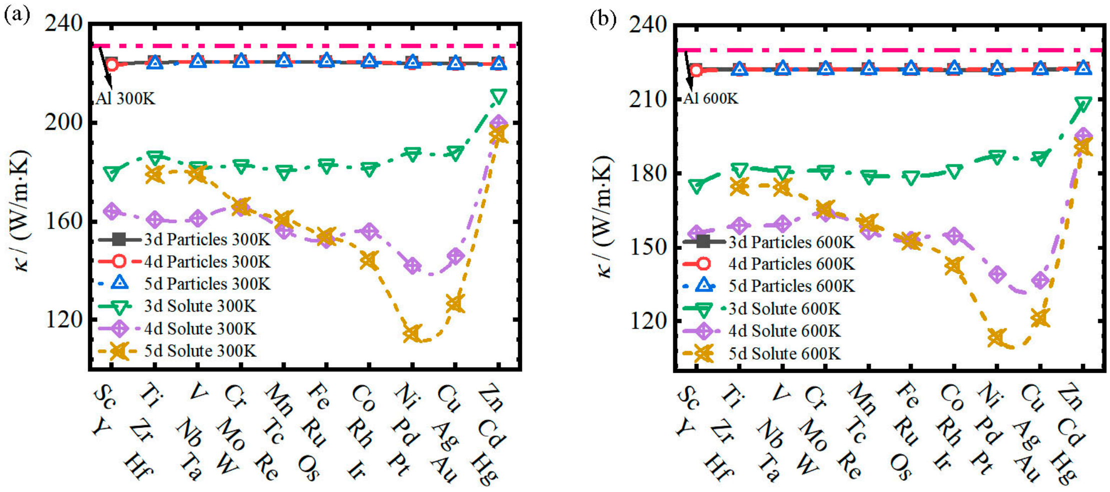

Figure 4. The calculated thermal conductivity κ of Al matrix by adding 1 at.% TM as a function of atomic number at (**a**) low and (**b**) high temperatures, respectively. The thermal conductivity of the pure Al matrix is plotted with a short-dashed line.

In summary, the effect of TM solute atoms on the thermal conductivity of Al is much greater than that of the second-phase particles, and the effect of Pd and Pt atoms is the most significant. The reason may be that the thermal conductivity of the second-phase particles is closer to the Al matrix and can retain the high thermal conductivity of the Al matrix to a greater extent.

4. Conclusions

In summary, based on first-principles calculations, the effect of substitution point defects TM_{Al} on the stability and thermal conductivity of aluminum was investigated. The main results show as follows:

1. The equilibrium lattice constant a_0 of Al-TM_{Al} supercells changes very little, while the defect formation energy of substitution defects TM_{Al} on the Al matrix exhibits a similar "W"-shaped periodic change with the increase in atomic number for 3d–5d TM elements. The E_f of TM_{Al} for both groups IB and IIB is greater than 0, indicating that these two subgroup elements are more difficult to form substitution defects in Al with. It is speculated that the valence electron structures of the elements play a crucial role.
2. The thermodynamic property parameters calculated with the Debye theory show that the addition of TM atoms can effectively reduce the thermal expansion coefficient of the material without changing the stability of the Al system, which provides support for the application of Al in the field of high-temperature precision instruments.
3. The ETC κ_e and the TC κ decrease at the temperature range of 100–200 K and then show a small variation. Moreover, because the lattice thermal conductivity κ_l has little effect, the electron TC κ_e and total TC of Al-TM_{Al} κ have the same linear increase trends with temperature. But all are slightly lower than that of a pure aluminum matrix.
4. At 300 K and 600 K, the total TC κ and the ETC κ_e for 3d TM increase slowly from Al-Sc_{Al} to Al-Cu_{Al} and then show a rapid increase to Al-Zn_{Al} with the increase in atomic number. The total TC κ in 4d (Y-Cd) and 5d (Hf-Hg) first drops slowly to Pd and Pt and then rises sharply after reaching the lowest point.
5. Finally, we chose to add 1 at.% TM to an Al matrix as $L1_2$ s phases and solute atoms at 300 K and 600 K. It was obviously found that the TC of the second-phase-containing Al matrix is slightly lower than that of pure aluminum, while the solute atoms TM_{Al} significantly reduce the thermal conductivity of the Al material. Therefore, the second phase should be favorable and must avoid solid solution atoms in the matrix from the point of view of thermal conductivity.

Supplementary Materials: The following supporting information can be downloaded at: https://www.mdpi.com/article/10.3390/cryst14010035/s1, Table S1. The calculated lattice thermal conductivity (LTC) κ_l ($Wm^{-1}k^{-1}$) of Al-TM_{Al} supercell at various temperatures, as plotted in Figure 2b; Table S2. The calculated electronic thermal conductivity (ETC) κ_l ($Wm^{-1}k^{-1}$) of Al-TM_{Al} supercell at various temperatures, as plotted in Figure 2d; Table S3. The calculated total thermal conductivity (TC) κ_l ($Wm^{-1}k^{-1}$) of Al-TM_{Al} supercell at various temperatures, as plotted in Figure 2d. Table S4. The calculated total thermal conductivity (TC) κ_l ($Wm^{-1}k^{-1}$) of the second phase particle $L1_2$-Al_3TM with 1% solute atoms TM added at 300 K and 600 K. Table S5. The calculated total thermal conductivity (TC) κ_l ($Wm^{-1}k^{-1}$) of Al-TM_{Al} solid solution with 1% solute atoms TM added at 300. Table S6. The optimized Al-W is taken as an example to export a copy of the extxyz file with lattice parameters and atomic positions.

Author Contributions: Conceptualization, T.F. and T.Y.; methodology, T.F.; software, T.F., L.L. and Z.R.; validation, L.L. and Z.R.; formal analysis, L.L., Z.R. and T.F.; investigation, L.L. and Z.R.; resources, T.Y., Z.R., Y.W. and D.C.; data curation, L.L., Z.R. and T.F.; writing—original draft preparation, L.L.; writing—review and editing, T.F.; visualization, L.L. and Z.R.; supervision, T.F., Y.W. and D.C.; project administration, T.Y., T.F., Y.W. and D.C.; funding acquisition, T.Y., T.F., Y.W. and D.C. All authors have read and agreed to the published version of the manuscript.

Funding: This research was funded by the Basic and Applied Basic Research Fund of Guangdong Province, grant number 2020B1515120093; the Natural Science Foundation of China, grant numbers 52201074, 52171115; and the Scientific Research Project of Hunan Institute of Technology, grant numbers HQ21016, 21A0564, HP21047, 2022SE090.

Data Availability Statement: The relevant data for this paper can be obtained from the article and the supplement.

Acknowledgments: We would like to thank the Guangdong Xiangqing Environmental Protection Technology Co., Ltd. and Foshan Fanxing Super-computing Network Technology Co., Ltd. for providing us the computing resources.

Conflicts of Interest: The authors declare no conflict of interest.

References

1. Wen, K.; Xiong, B.Q.; Fan, Y.Q.; Zhang, Y.A.; Li, Z.H.; Li, X.W.; Wang, F.; Liu, H.W. Transformation and dissolution of second phases during solution treatment of an Al–Zn–Mg–Cu alloy containing high zinc. *Rare Met.* **2018**, *37*, 376–380. [CrossRef]
2. Mulyawan, A.; Terai, T.; Fukuda, T. Interpretation of Fe-rich part of Fe–Al phase diagram from magnetic properties of A2-, B2-, and DO3-phases. *J. Alloys Compd.* **2020**, *834*, 155140. [CrossRef]
3. Oropeza, D.; Hofmann, D.C.; Williams, K.; Firdosy, S.; Bordeenithikasem, P.; Sokoluk, M.; Liese, M.; Liu, J.; Li, X. Welding and additive manufacturing with nanoparticle-enhanced aluminum 7075 wire. *J. Alloys Compd.* **2020**, *834*, 154987. [CrossRef] [PubMed]
4. Dhakal, B.; Swaroop, S. Effect of laser shock peening on mechanical and microstructural aspects of 6061-T6 aluminum alloy. *J. Mater. Process. Tech.* **2020**, *282*, 116640. [CrossRef]
5. Ma, H.; Zhang, X.; Liu, C.; Zhao, L.; Jiang, W. Structural, elastic, anisotropic and thermodynamic properties of the caged intermetallics RETi2Al20 (RE = La, Ce, Gd and Ho): A first-principles study. *Solid State Sci.* **2019**, *89*, 121–129. [CrossRef]
6. Schlapbach, L.; Züttel, A. Hydrogen-storage materials for mobile applications. *Nature* **2001**, *414*, 353–358. [CrossRef] [PubMed]
7. Zhang, A.; Li, Y. Effect of alloying elements on thermal conductivity of aluminum. *J. Mater. Res.* **2023**, *38*, 2049–2058. [CrossRef]
8. Chen, J.K.; Hung, H.Y.; Wang, C.F.; Tang, N.K. Thermal and electrical conductivity in Al–Si/Cu/Fe/Mg binary and ternary Al alloys. *J. Mater. Sci.* **2015**, *50*, 5630–5639. [CrossRef]
9. Gan, J.Q.; Huang, Y.J.; Cheng, W.E.; Jun, D.U. Effect of Sr modification on microstructure and thermal conductivity of hypoeutectic Al−Si alloys. *Trans. Nonferrous Met. Soc. China* **2020**, *30*, 2879–2890. [CrossRef]
10. Liu, S.; Wang, S.; Zhang, B.; Zhang, X.; Ma, M.; Liu, R. Dynamic precipitation-induced simultaneous enhancement of the strength and plasticity of hot-rolled Zr–9Al alloy. *J. Alloys Compd.* **2020**, *829*, 154577.
11. Li, M.; Li, H.; Zhang, Z.; Shi, W.; Liu, J.; Hu, Y.; Wu, Y. Effect of precipitates on properties of cold-rolled Al–Mg–Si–Sc–Zr alloy with higher temperature aging. *Mater. Sci. Technol.* **2018**, *34*, 1246–1251. [CrossRef]
12. Ohara, S.; Chen, G.; Sakamoto, I. Effect of pressure on transport properties of mixed-valence compound $YbAl_3$. *J. Alloys Compd.* **2001**, *323*, 632–635. [CrossRef]
13. Taendl, J.; Orthacker, A.; Amenitsch, H.; Kothleitner, G.; Poletti, C. Influence of the degree of scandium supersaturation on the precipitation kinetics of rapidly solidified Al-Mg-Sc-Zr alloys. *Acta Mater.* **2016**, *117*, 43–50. [CrossRef]
14. Yu, L.; Wang, J.; Qu, F.; Wang, M.; Wang, W.; Bao, Y.; Lai, X. Effects of scandium addition on microstructure, mechanical and thermal properties of cast Be-Al alloy. *J. Alloys Compd.* **2018**, *737*, 655–664. [CrossRef]

15. Suwanpreecha, C.; Pandee, P.; Patakham, U.; Limmaneevichitr, C. New generation of eutectic Al-Ni casting alloys for elevated temperature services. *Mater. Sci. Eng. A* **2018**, *709*, 46–54. [CrossRef]
16. Dorin, T.; Ramajayam, M.; Lamb, J.; Langan, T. Effect of Sc and Zr additions on the microstructure/strength of Al-Cu binary alloys. *Mater. Sci. Eng. A* **2017**, *707*, 58–64. [CrossRef]
17. Tian, T.; Wang, X.; Li, W. Ab initio calculations on elastic properties in $L1_2$ structure Al_3X and X_3Al-type (X=transition or main group metal) intermetallic compounds. *Solid State Commun.* **2013**, *156*, 69–75. [CrossRef]
18. Seidman, D.N.; Marquis, E.A.; Dunand, D.C. Precipitation strengthening at ambient and elevated temperatures of heat-treatable Al(Sc) alloys. *Acta Mater.* **2002**, *50*, 4021–4035. [CrossRef]
19. Iwamura, S.; Miura, Y. Loss in Coherency and Coarsening Behavior of Al_3Sc precipitates. *Acta Mater.* **2004**, *52*, 591–600. [CrossRef]
20. Mikhaylovskaya, A.; Mochugovskiy, A.; Levchenko, V.; Tabachkova, N.; Mufalo, W.; Portnoy, V. Precipitation behavior of L12 Al_3Zr phase in Al-Mg-Zr alloy. *Mater. Charact.* **2018**, *139*, 30–37. [CrossRef]
21. Chen, Z.; Zhang, P.; Chen, D.; Wu, Y.; Wang, M.; Ma, N.; Wang, H. First-principles investigation of thermodynamic, elastic and electronic properties of Al_3V and Al_3Nb intermetallics under pressures. *J. Appl. Phys.* **2015**, *117*, 085904. [CrossRef]
22. Wen, S.P.; Wang, W.; Zhao, W.H.; Wu, X.L.; Gao, K.Y.; Huang, H.; Nie, Z.R. Precipitation hardening and recrystallization behavior of AlMgErZr alloys. *J. Alloys Compd.* **2016**, *687*, 143–151. [CrossRef]
23. Lin, J.D.; Okle, P.; Dunand, D.C.; Seidman, D.N. Effects of Sb micro-alloying on precipitate evolution and mechanical properties of a dilute Al-Sc-Zr alloy. *Mater. Sci. Eng. A* **2017**, *680*, 64–74. [CrossRef]
24. Vo, N.Q.; Dunand, D.C.; Seidman, D.N. Improving aging and creep resistance in a dilute Al–Sc alloy by microalloying with Si, Zr and Er. *Acta Mater.* **2014**, *63*, 73–85. [CrossRef]
25. Clouet, E.; Barbu, A.; Laé, L.; Martin, G. Precipitation kinetics of Al_3Zr and Al_3Sc in aluminum alloys modeled with cluster dynamics. *Acta Mater.* **2005**, *53*, 2313–2325. [CrossRef]
26. Hyde, K.; Norman, A.; Prangnell, P. The effect of cooling rate on the morphology of primary Al_3Sc intermetallic particles in Al–Sc alloys. *Acta Mater.* **2001**, *49*, 1327–1337. [CrossRef]
27. Lee, S.; Utsunomiya, A.; Akamatsu, H.; Neishi, K.; Furukawa, M.; Horita, Z.; Langdon, T. Influence of scandium and zirconium on grain stability and superplastic ductilities in ultrafine-grained Al–Mg alloys. *Acta Mater.* **2002**, *50*, 553–564. [CrossRef]
28. Oku, M.; Shishido, T.; Sun, Q.; Nakajima, K.; Kawazoe, Y.; Wagatsuma, K. Comparison of electronic structures of $ScAl_3$ and ScRh3: X-ray photoelectron spectroscopy and ab initio band calculation. *J. Alloys Compd.* **2003**, *358*, 264–267. [CrossRef]
29. Jahnátek, M.; Krajčí, M.; Hafner, J. Interatomic bonding, elastic properties, and ideal strength of transition metal aluminides: A case study for Al_3(V, Ti). *Phys. Rev. B* **2005**, *71*, 024101. [CrossRef]
30. Radmilovic, V.; Ophus, C.; Marquis, E.A.; Rossell, M.D.; Tolley, A.; Gautam, A.; Asta, M.; Dahmen, U. Highly monodisperse core–shell particles created by solid-state reactions. *Nat. Mater.* **2011**, *10*, 710–715. [CrossRef]
31. Wang, Y.; Wang, J.; Zhang, C.; Huang, H. Mechanical properties of defective $L1_2$-Al_3X (X= Sc, Lu) phase: A first-principles study. *J. Rare Earths* **2021**, *39*, 217–224. [CrossRef]
32. Hu, W.-C.; Liu, Y.; Li, D.-J.; Zeng, X.-Q.; Xu, C.-S. Mechanical and thermodynamic properties of Al_3Sc and Al_3Li precipitates in Al–Li–Sc alloys from first-principles calculations. *Physica B* **2013**, *427*, 85–90. [CrossRef]
33. Mondolfo, L.F. *Aluminum Alloys: Structure and Properties*; Elsevier: Amsterdam, The Netherlands, 2013.
34. Nakamura, M.; Kimura, K. Elastic constants of $TiAl_3$ and $ZrAl_3$ single crystals. *J. Mater. Sci.* **1991**, *26*, 2208–2214. [CrossRef]
35. Umakoshi, Y.; Yamaguchi, M.; Sakagami, T.; Yamane, T. Oxidation resistance of intermetallic compounds Al_3Ti and TiAl. *J. Mater. Sci.* **1989**, *24*, 1599–1603. [CrossRef]
36. Aguilar-Virgen, J.; Cabrera, A.; Umemoto, M.; Calderón, H. Compressive mechanical properties of nanostructured intermetallic alloys Al_3Ti-X (X = Mn or Fe). *Mater. Sci. Forum* **2006**, *509*, 63–68. [CrossRef]
37. Fu, Y.; Shi, R.; Zhang, J.; Sun, J.; Hu, G. Microstructure and mechanical behavior of a multiphase Al_3Ti-based intermetallic alloy. *Intermetallics* **2000**, *8*, 1251–1256. [CrossRef]
38. Guan, R.; Shen, Y.; Zhao, Z.; Wang, X. A high-strength, ductile Al-0.35 Sc-0.2 Zr alloy with good electrical conductivity strengthened by coherent nanosized-precipitates. *J. Mater. Sci. Technol.* **2017**, *33*, 215–223. [CrossRef]
39. Wen, S.P.; Xing, Z.B.; Huang, H.; Li, B.L.; Wang, W.; Nie, Z.R. The effect of erbium on the microstructure and mechanical properties of Al-Mg-Mn-Zr alloy. *Mater. Sci. Eng. A* **2009**, *516*, 42–49. [CrossRef]
40. Xiaoyuan, W.E.; Huang, H.; Ziyong, C.H.; Wei, W.A.; Congying, L.I.; Zuoren, N.I. Microstructure and mechanical properties of Al-Mg-Mn-Zr-Er weld joints filled with Al-Mg-Mn-Zr and Al-Mg-Mn-Zr-Er weld wires. *J. Rare Earths* **2010**, *28*, 627–630.
41. Wen, S.; Gao, K.; Li, Y.; Huang, H.; Nie, Z. Synergetic effect of Er and Zr on the precipitation hardening of Al-Er-Zr alloy. *Scr. Mater.* **2011**, *65*, 592–595. [CrossRef]
42. Koutná, N.; Erdely, P.; Zöhrer, S.; Franz, R.; Du, Y.; Liu, S.; Mayrhofer, P.H.; Holec, D. Experimental chemistry and structural stability of AlNb3 enabled by antisite defects formation. *Materials* **2019**, *12*, 1104. [CrossRef] [PubMed]
43. Valkov, S.; Petrov, P.; Lazarova, R.; Bezdushnyi, R.; Dechev, D. Formation and characterization of Al–Ti–Nb alloys by electron-beam surface alloying. *Appl. Surf. Sci.* **2016**, *389*, 768–774. [CrossRef]
44. Nong, Z.; Zhu, J.; Yang, X.; Cao, Y.; Lai, Z.; Liu, Y. The mechanical, thermodynamic and electronic properties of Al_3Nb with DO22 structure: A first-principles study. *Physica B* **2012**, *407*, 3555–3560. [CrossRef]

45. Zhang, X.; Dong, T.; Ma, H.; Li, D.; Ying, C.; Liu, C.; Wang, F. A first principles investigation on the influence of transition-metal elements on the structural, mechanical, and anisotropic properties of CaM_2Al_{20} intermetallics. *J. Mol. Graph. Model.* **2020**, *96*, 107509. [CrossRef] [PubMed]
46. Saha, S.; Todorova, T.Z.; Zwanziger, J.W. Temperature dependent lattice misfit and coherency of Al_3X (X = Sc, Zr, Ti and Nb) particles in an Al matrix. *Acta Mater.* **2015**, *89*, 109–115. [CrossRef]
47. Tzeng, Y.-C.; Chung, C.-Y.; Chien, H.-C. Effects of trace amounts of Zr and Sc on the recrystallization behavior and mechanical properties of Al-4.5 Zn-1.6 Mg alloys. *Mater. Lett.* **2018**, *228*, 270–272. [CrossRef]
48. Krug, M.E.; Mao, Z.; Seidman, D.N.; Dunand, D.C. Comparison between dislocation dynamics model predictions and experiments in precipitation-strengthened Al–Li–Sc alloys. *Acta Mater.* **2014**, *79*, 382–395. [CrossRef]
49. Sheng, B.; Niu, M.; Shao, X. Conductivity and magnetic properties study on doped semiconductor material of 3C-SiC: A first-principle investigation. In Proceedings of the IEEE International Conference on Electric Information and Control Engineering, Wuhan, China, 15–17 April 2011; pp. 5758–5761.
50. Majid, A.; Rani, N.; Khan, S.U.-D.; Almutairi, Z.A. First principles study of structural, electronic and magnetic properties of transition metals doped SiC monolayers for applications in spintronics. *J. Magn. Magn. Mater.* **2020**, *503*, 166648. [CrossRef]
51. Cao, Z.; Jin, N.; Ye, J.; Du, X.; Liu, Y. First-principles study on the effects of N and Al doping on the mechanical properties and electronic structures of TiC. *RSC Adv.* **2020**, *10*, 36295–36302. [CrossRef]
52. Rajasekar, P.; Umarji, A.M. Effect of Al-doping on suppression of thermal conductivity in Si dispersed β-$FeSi_2$. *Intermetallics* **2017**, *89*, 57–64. [CrossRef]
53. Vandersluis, E.; Lombardi, A.; Ravindran, C.; Bois-Brochu, A.; Chiesa, F.; MacKay, R. Factors influencing thermal conductivity and mechanical properties in 319 Al alloy cylinder heads. *Mater. Sci. Eng. A* **2015**, *648*, 401–411. [CrossRef]
54. Hafner, J. Ab-initio simulations of materials using VASP: Density-functional theory and beyond. *J. Comput. Chem.* **2008**, *29*, 2044–2078. [CrossRef] [PubMed]
55. Maruhn, J.A.; Reinhard, P.G.; Suraud, E. *Density Functional Theory*; Plenum Press: New York, NY, USA, 2010.
56. Perdew, J.P.; Burke, K.; Ernzerhof, M. Generalized Gradient Approximation Made Simple. *Phys. Rev. Lett.* **1996**, *77*, 3865–3868. [CrossRef] [PubMed]
57. Monkhorst, H.J.; Pack, J.D. Special points for Brillouin-zone integrations. *Phys. Rev. B* **1976**, *13*, 5188–5192. [CrossRef]
58. Feynman, R.P. Forces in Molecules. *Phys. Rev.* **1939**, *56*, 340. [CrossRef]
59. Madsen, G.K.; Carrete, J.; Verstraete, M.J. BoltzTraP2, a program for interpolating band structures and calculating semi-classical transport coefficients. *Comput. Phys. Commun.* **2018**, *231*, 140–145. [CrossRef]
60. Debye, P. Zur theorie der spezifischen wärmen. *Annalen der Physik* **1912**, *344*, 789–839. [CrossRef]
61. Khenioui, Y.; Boulechfar, R.; Maazi, N.; Ghemid, S. FP-LAPW investigation of $Al_3(Sc_{1x}Ti_x)$ alloys properties in $L1_2$ and $D0_{22}$ structures. *Int. J. Mod. Phys. B* **2018**, *32*, 1850167. [CrossRef]
62. Tao, X.; Ouyang, Y.; Liu, H.; Zeng, F.; Feng, Y.; Jin, Z. Calculation of the thermodynamic properties of B2 AlRE (RE = Sc, Y, La, Ce–Lu). *Physica B* **2007**, *399*, 27–32. [CrossRef]
63. Fu, H.; Zhao, Z.; Liu, W.; Peng, F.; Gao, T.; Cheng, X. Ab initio calculations of elastic constants and thermodynamic properties of γTiAl under high pressures. *Intermetallics* **2010**, *18*, 761–766. [CrossRef]
64. Zhang, S.B.; Northrup, J.E. Chemical potential dependence of defect formation energies in GaAs: Application to Ga self-diffusion. *Phys. Rev. Lett.* **1991**, *67*, 2339. [CrossRef]
65. Dong, T.H.; Zhang, X.D.; Yang, L.M.; Wang, F. An effect of structural vacancies on the lattice vibration, mechanical, electronic and thermodynamic properties of Cr_5BSi_3. *Chin. Phys. B* **2021**, *31*, 026101. [CrossRef]
66. Qiu, R.; Lu, H.; Ao, B.; Huang, L.; Tang, T.; Chen, P. Energetics of intrinsic point defects in aluminium via orbital-free density functional theory. *Philos. Mag.* **2017**, *97*, 2164–2181. [CrossRef]
67. Bandyopadhyay, J.; Gupta, K. Low temperature lattice parameters of Al and Al-Zn alloys and Grüneisen parameter of Al. *Cryogenics* **1978**, *18*, 54–55. [CrossRef]
68. Ehrhart, P. *Atomic Defects in Metals*; Springer: Berlin/Heidelberg, Germany, 1991.
69. Carling, K.; Wahnström, G.; Mattsson, T.R.; Mattsson, A.E.; Sandberg, N.; Grimvall, G. Vacancies in Metals: From First-Principles Calculations to Experimental Data. *Phys. Rev. Lett.* **2000**, *85*, 3862. [CrossRef] [PubMed]
70. Chen, X.R.; Zeng, Z.Y.; Liu, Z.L.; Cai, L.C.; Jing, F.Q. Elastic anisotropy of ε-Fe under conditions at the Earth's inner core. *Phys. Rev. B* **2011**, *83*, 132102. [CrossRef]
71. Deng, L.; Liu, X.; Liu, H.; Dong, J. High-pressure phase relations in the composition of albite $NaAlSi_3O_8$ constrained by an ab initio and quasi-harmonic Debye model, and their implications. *Earth Planet. Sci. Lett.* **2010**, *298*, 427–433. [CrossRef]
72. Errandonea, D.; Kumar, R.S.; Gracia, L.; Beltran, A.; Achary, S.N.; Tyagi, A.K. Experimental and theoretical investigation of $ThGeO_4$ at high pressure. *Phys. Rev. B* **2009**, *80*, 094101. [CrossRef]
73. Chen, Y.; Hammerschmidt, T.; Pettifor, D.; Shang, J.-X.; Zhang, Y. Influence of vibrational entropy on structural stability of Nb–Si and Mo–Si systems at elevated temperatures. *Acta Mater.* **2009**, *57*, 2657–2664. [CrossRef]
74. Ayad, M.; Belkharroubi, F.; Boufadi, F.Z.; Khorsi, M.; Zoubir, M.K.; Ameri, M.; Ameri, I.; Al-Douri, Y.; Bidai, K.; Bensaid, D. First-principles calculations to investigate magnetic and thermodynamic properties of new multifunctional full-Heusler alloy Co_2TaGa. *Indian J. Phys.* **2020**, *94*, 767–777. [CrossRef]

75. Hadji, S.; Bouhemadou, A.; Haddadi, K.; Cherrad, D.; Khenata, R.; Bin-Omran, S.; Al-Douri, Y. Elastic, electronic, optical and thermodynamic properties of Ba3Ca2Si2N6 semiconductor: First-principles predictions. *Phys. B Condens. Matter* **2020**, *589*, 412213. [CrossRef]
76. Anderson, O. Determination and some uses of isotropic elastic constants of polycrystalline aggregates using single-crystal data. In *Physical Acoustics*; Elsevier: Amsterdam, The Netherlands, 1965; pp. 43–95.
77. Mallick, P.K. *Materials, Design and Manufacturing for Lightweight Vehicles*; CRC Press: Boca Raton, FL, USA, 2010.
78. Takahashi, K.; Kuwahara, H.; Kawasaki, N.; Obata, T.; Sugawa, E. Enhancement of Thermal Contact Conductance Between Metal Surfaces in an Induction Motor. *J. Enhanc. Heat Transf.* **2001**, *8*, 201–213. [CrossRef]
79. Jain, A.; McGaughey, A.J.H. Thermal transport by phonons and electrons in aluminum, silver, and gold from first principles. *Phys. Rev. B* **2016**, *93*, 081206. [CrossRef]
80. Jossou, E.; Malakkal, L.; Szpunar, B.; Oladimeji, D.; Szpunar, J.A. A first principles study of the electronic structure, elastic and thermal properties of UB2. *J. Nucl. Mater.* **2017**, *490*, 41–48. [CrossRef]
81. Togo, A.; Chaput, L.; Tanaka, I.; Hug, G. First-principles phonon calculations of thermal expansion in Ti_3SiC_2, Ti_3AlC_2, and Ti_3GeC_2. *Phys. Rev. B* **2010**, *81*, 174301. [CrossRef]
82. Wang, Y.; Ohishi, Y.; Kurosaki, K.; Muta, H. First-principles calculation study of Mg_2XH_6 (X = Fe, Ru) on thermoelectric properties. *Mater. Res. Express* **2019**, *6*, 085536. [CrossRef]
83. Slack, G.A. Nonmetallic crystals with high thermal conductivity. *J. Phys. Chem. Solids* **1973**, *34*, 321–335. [CrossRef]
84. Madsen, G.K.; Singh, D.J. BoltzTraP. A code for calculating band-structure dependent quantities. *Comput. Phys. Commun.* **2006**, *175*, 67–71. [CrossRef]
85. Yadav, M.K.; Sanyal, B. First principles study of thermoelectric properties of Li-based half-Heusler alloys. *J. Alloys Compd.* **2015**, *622*, 388–393. [CrossRef]
86. Mubashir, S.; Butt, M.K.; Yaseen, M.; Iqbal, J.; Iqbal, M.; Murtaza, A.; Laref, A. Pressure induced electronic, optical and thermoelectric properties of cubic $BaZrO_3$: A first principle Calculations. *Opt. Int. J. Light Electron Opt.* **2021**, *239*, 166694. [CrossRef]
87. Remil, G.; Zitouni, A.; Bouadjemi, B.; Houari, M.; Abbad, A.; Benstaali, W.; Cherid, S.; Matougui, M.; Lantri, T.; Bentata, S. A potential full Heusler thermoelectric material CO_2ZrZ (Z =Al, Si, Ga and Sn) in low temperature: An Ab-initio investigation. *Solid State Commun.* **2021**, *336*, 114422. [CrossRef]
88. Brandt, R.; Neuer, G. Electrical Resistivity and Thermal Conductivity of Pure Aluminum and Aluminum Alloys up to and above the Melting Temperature. *Int. J. Thermophys.* **2007**, *28*, 1429–1446. [CrossRef]
89. Powell, R.W. Correlation of metallic thermal and electrical conductivities for both solid and liquid phases. *Int. J. Heat Mass Transf.* **1965**, *8*, 1033–1045. [CrossRef]
90. De Lang, H.N.; van Kempen, H.; Wyder, P. The lattice thermal conductivity of very pure aluminium. *J. Phys. F Met. Phys.* **1978**, *8*, L39. [CrossRef]
91. Ahmad, S.; Mahanti, S.D. Energy and temperature dependence of relaxation time and Wiedemann-Franz law on PbTe. *Phys. Rev. B* **2010**, *81*, 165203. [CrossRef]
92. Choi, G.; Kim, H.S.; Lee, K.; Park, S.H.; Cha, J.; Chung, I.; Lee, W.B. Study on thermal conductivity and electrical resistivity of Al-Cu alloys obtained by Boltzmann transport equation and first-principles simulation: Semi-empirical approach. *J. Alloys Compd.* **2017**, *727*, 1237–1242. [CrossRef]
93. Wen, B.; Feng, X. Thermal conductivity of metal from first principles calculations and its application in aluminum. *J. Yanshan Univ.* **2015**, *39*, 298–306.